Chinese Chemical Letters 34 (2023) 107865

Contents lists available at ScienceDirect

Chinese Chemical Letters

journal homepage: www.elsevier.com/locate/cclet

Design and characterizing of robust probes for enhanced mass spectrometry imaging and spatially resolved metabolomics

Jianpeng Huang[a,b,1], Shanshan Gao[a,b,1], Kai Wang[c], Jin Zhang[a,b], Xuechao Pang[a,b], Junwen Shi[c,*], Jiuming He[a,b,*]

[a] State Key Laboratory of Bioactive Substance and Function of Natural Medicines, Institute of Materia Medica, Chinese Academy of Medical Sciences and Peking Union Medical College, Beijing 100050, China
[b] NMPA Key Laboratory of Safety Research and Evaluation of Innovative Drug, Institute of Materia Medica, Chinese Academy of Medical Sciences and Peking Union Medical College, Beijing 100050, China
[c] Viktor Technology Co., Ltd., Beijing 101100, China

ARTICLE INFO

Article history:
Received 29 April 2022
Revised 13 September 2022
Accepted 27 September 2022
Available online 1 October 2022

Keywords:
Air-flow assisted desorption electrospray ionization
Mass spectrometry imaging
Molecular imaging
Spatially resolved metabolomics
Brain

ABSTRACT

As for the emerging and cut edge spatially resolved metabolomics, mass spectrometry imaging (MSI) is a powerful tool that can map thousands of metabolites from bio-tissue sections without chemical labels. However, the stability, sensitivity and spatial resolution of MSI are always limited by the performance of its ionization probe. Herein, two types of probes (fine probe (P-100) and large probe (P-200)) were designed and characterized to perform air-flow assisted desorption electrospray ionization (AFA-DESI) MSI analysis for spatially resolved metabolomics. It was determined that the spray introduced by P-100 was homogenous and stable under the spray solvent at a flow rate of 5-10 μL/min, while P-200 can endure a high flow rate of up to 10-30 μL/min. Moreover, the MSI images were acquired by AFA-DESI-MSI with P-100 from rat brain tissue section and with P-200 from whole-body tissue section of mouse, and these results presented unambiguous tissue structure with the distribution information of numerous metabolites. Furthermore, the spatially resolved metabolomic analysis of tumor tissue was successfully realized to discover the tumor associated biomarkers. As the key parts of AFA-DESI-MSI system, it has been demonstrated that the designed probs have excellent performance for spatially resolved metabolomics, and it will further promote its application in life science, and drug research and development.

Spatially resolved metabolomics has received widespread attention in recent years because of its unique ability to reflect three-dimensional omics information to understand complex biological processes [1]. As the dominant technology for spatially resolved metabolomic analysis, mass spectrometry imaging (MSI) enables the ability to characterize the spatial distribution of diverse compounds on complex surfaces without tedious sample processing [2–4]. Various in situ ionization technologies (that is, probes) are used in MSI to directly scan and ionize biological tissue samples by position, followed by mass spectrometry analysis. The combinatorial information of *m*/*z*, intensity, and localization of thousands of metabolites can be acquired simultaneously within a single detection. MSI has been widely used in spatial distribution and relative abundance analysis of multiple endogenous and exogenous molecules in biological tissues, including proteins, metabolites, lipids and drugs [5–9]. Compared with traditional histological analysis techniques, such as immunohistochemistry, immunofluorescence, and radioisotope labeling, MSI is not limited to one or more specific molecular species, and thousands of compounds can be detected without any chemical modification or labeling before analysis [10,11]. Therefore, MSI technology-based spatially resolved metabolomics has extensive application prospects in clinical medicine [12,13], life sciences [14–16], new drug research and development [17] and botany [18].

Divided by ionization technology, the most frequently used MSI methods include matrix-assisted laser desorption ionization (MALDI), secondary ion mass spectrometry (SIMS), and desorption electrospray ionization (DESI) [19]. SIMS, used in MSI as early as 50 years ago [20], can reach the highest spatial resolution of 50-100 nm [21], but it is more suitable for elemental analysis due to its high energy and strong destructive characteristics [22,23]. MALDI-MSI is currently a widely used probe technology in MSI [24,25] and can achieve the analysis of molecules with a broad mass range and minimum spatial resolution of 5 μm [26,27]. How-

* Corresponding authors.
E-mail addresses: apsorc@aliyun.com (J. Shi), hejiuming@imm.ac.cn (J. He).
[1] These authors contributed equally to this work.

https://doi.org/10.1016/j.cclet.2022.107865
1001-8417/

ever, the presence of a matrix is likely to cause problems such as spatial displacement of the analyte and interference of endogenous small molecules [28], causing low sensitivity due to the lack of solvent extraction [29]. Compared with SIMS-MSI and MALDI-MSI for analysis under vacuum, DESI-MSI is an ambient ionization imaging technology that has been developed into a relatively fast and simple technology for direct analysis of complex surfaces without matrix interference and with a spatial resolution of 50-100 μm [30–32]. Based on DESI-MSI, our group proposed and realized an air-flow assisted DESI-MSI (AFA-DESI-MSI) technique [5,33,34]. Charged droplets are transported over a long distance through the transmission tube, where they are further desolvated, enriched, and ionized under the presence of high-speed air flow and voltage. This process can improve detection sensitivity and operational flexibility, making it suitable for MSI analysis of large-volume samples. Based on AFA-DESI-MSI analysis, we achieved high-sensitivity, high-coverage imaging analysis of endogenous metabolites in biological tissues [35–37] and *in situ* characterization of drugs and metabolites in whole-body animals [19]. This technique provides a novel and intuitive quantitative method for drug research and development [38–40], tumor pathological diagnosis [41–43], and tumor metabolism research [44].

Clarifying the high-resolution spatial distribution of functional molecules is essential for elucidating their biological or pharmacological effects [10]. However, it is well known that an inverse relationship exists between sensitivity and spatial resolution. The high resolution of SIMS and MALDI comes at the expense of sensitivity due to reduced sample desorption [3]. Therefore, the trade-off between sensitivity and resolution has always been a problem that urgently needs to be solved in MSI analysis. Desorption ionization is the leading process to realize MSI analysis, and the performance of electrospray ionization probes of ambient MSI has a greater impact on sensitivity, resolution, and imaging quality [45]. We look forward to improving the sensitivity of MSI from the perspective of probes and achieving high coverage, high-resolution metabolite imaging for spatially resolved metabolomics, especially low-content functional metabolites in biological tissues.

In this work, based on the basic principle of AFA-DESI-MSI, new desorption electrospray probes were designed and characterized for its mass spectrometry imaging analysis performance, and then was applied in the spatially resolved metabolomics analysis of rat brain, tumor tissue and whole-body section. The results show that a stable and reliable desorption ionization effect can be obtained by using these probes, and high-sensitivity, reasonable spatial resolution and high quality mass spectrometry imaging analysis can be realized for spatially resolved metabolomics research.

Animals and samples: The animal experiments were approved by the Animal Care & Welfare Committee (Institute of Materia Medica, Chinese Academy of Medical Sciences and Peking Union Medical College). The whole brain of Sprague−Dawley rats was removed, placed on ice, and then washed with cold saline. The brains were stored at −80 °C and then were cut into 20 μm consecutive sagittal slices. The slices of brains were used to characterize the performance of the probe. BALB/C mice were inoculated subcutaneously with A549 lung cancer cell suspension mixed with Matrigel to establish the ectopic tumor model. After 2 weeks of inoculation, tumors were collected and intact whole-body were kept, stored in a refrigerator at −80 °C. The tumor tissue was cut into sections of 15 μm with a cryostat microtome for AFA-DESI-MSI analysis. BALB/c mice carcasses were embedded in a freezing block with 2.5% (w/v, g/100 mL) aqueous carboxymethyl cellulose. Twenty-five-micrometer-thick whole-body animal sagittal cryosections were made using a Leica CM 3600 XP instrument for AFA-DESI-MSI analysis. Detail of experimental methods was presented in Supporting information.

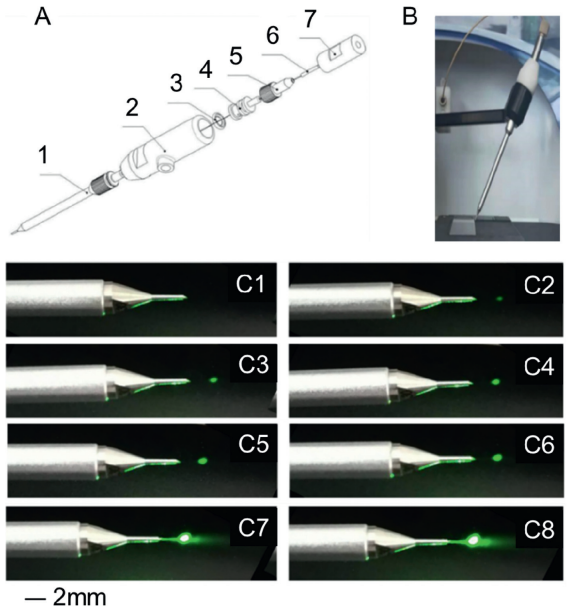

Fig. 1. (A) The structure of the designed desorption electrospray ionization probe. (1) Adjustable nozzle, (2) subject, (3) O-ring, (4) inner cavity, (5) PEEK connector, (6) capillary tube, (7) stainless steel union. (B) A photo of the probe assembled on the imaging platform. (C) Performance characterization of P-100 at flow rates of 0-20 μL/min. Flow rate (μL/min): (C1) 0; (C2) 1; (C3) 3; (C4) 5; (C5) 7; (C6) 10; (C7) 15; (C8) 20. The green dot represents the actual shape and size of the spray points.

Design of desorption electrospray probe: The same basic structure of fine probe (P-100) and large probe (P-200) were designed based on the fast-nebulizing gas jet. As shown in Fig. 1A, both probes were composed of an adjustable nozzle, a subject, an O-ring, a lumen, a PEEK connector, an inner capillary, and a stainless-steel union. The subject of the probe was designed with a high-pressure gas source connector, through which the nebulizing gas was introduced. One end of the capillary tube was fixed to the stainless-steel union through a PEEK connector, and the other end passed through the inner cavity and the subject to the probe nozzle. The length of the capillary tube protruding from the nozzle could be adjusted by rotating the adjusting nut. The picture of the probe assembled and installed on the AFA-DESI-MSI platform is shown in Fig. 1B. In order to generated high speed charged droplet for desorption ionization, the subject and the inner cavity are sealed by an O-ring, and high-pressure gas flows was introduced from the small holes in the inner cavity and along the coaxial direction of the capillary, and then out of the spray nozzle. The spray solvent is delivered through the stainless-steel union by an external microsyringe pump, and then it flows out through the inner capillary and forms spray under the action of high-pressure gas flow. The two types of probes differ only in the inner diameter of the capillary tube and the matching nozzle. The 100-type fine probe uses a 100 μm inner diameter capillary and its matching spray nozzle; the 200-type large-size probe uses a 200 μm inner diameter capillary and matching spray nozzle.

Characterizing the performance of the probes by photomicrographs: Fig. 1C shows the spray characteristics of the P-100 probe at different solvent flow rates. For P-100, the spray point size of 1 μL/min was approximately 100 μm, which increased with a higher solvent flow rate. The formed spray was stable and uniform with excellent dispersibility in the flow rate range of 1-10 μL/min. Conversely, at a higher flow rate of 20 μL/min, incomplete nebulization can cause solvent liquid accumulation on the sample surface, which will affect the performance of MSI. P-200 showed different characteristics and adaptability, and the spray stability was

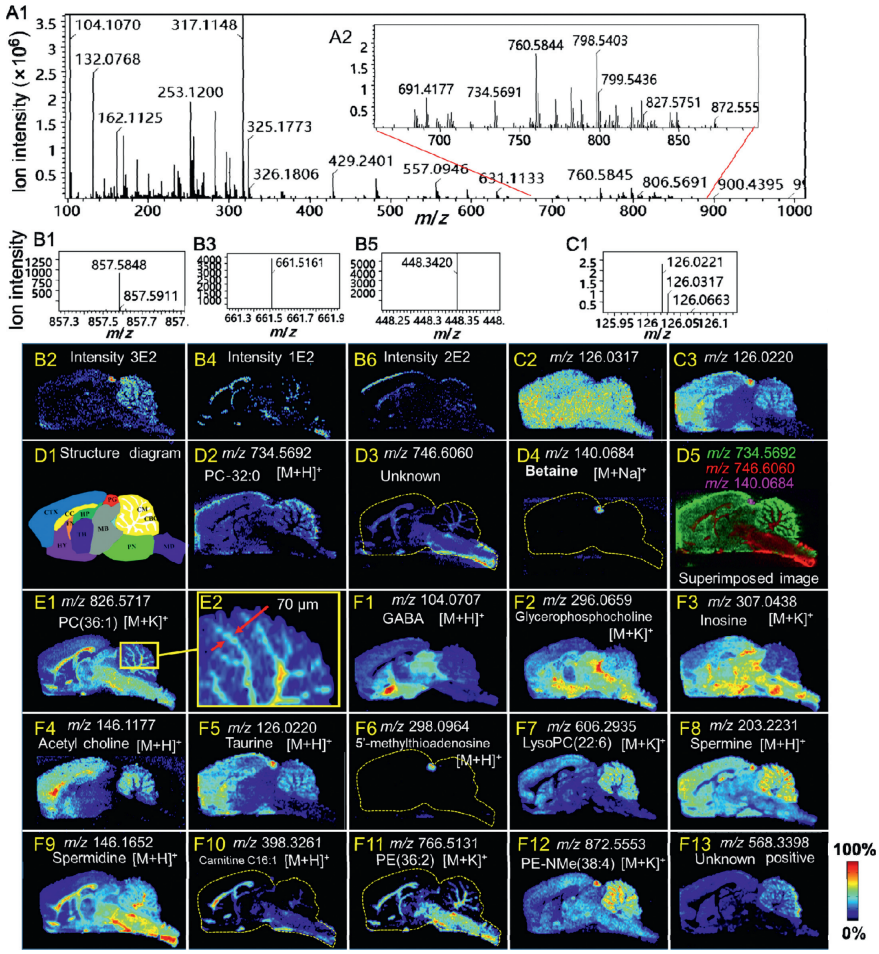

Fig. 2. AFA-DESI-MSI analytical results of rat brains using the P-100 probe. (A) Typical MS spectra from the rat brain. (B) MS spectra and images of low-abundance ions. (C) MS spectra and images of closed *m*/*z* ions. (D-F) MS images of representative metabolites in the rat brain. CTX, cerebral cortex; CC, corpus callosum; FN, fornix; HP, hippocampus; PG, pineal gland; HY, hypothalamus; TH, thalamus; MB, middle brain; CM, cerebellar medulla; CBC, cerebellar cortex; PN, pons; MD, medulla.

slightly poor at low flow rates of 1-3 μL/min, which was not conducive to fine MSI analysis. However, in the range of a large flow rate of 10-30 μL/min (Fig. S1 in Supporting information), this probe showed outstanding stability and droplet dispersion, which was suitable for rapid scanning and imaging of large samples.

MSI and spatially resolved metabolomics analysis using P-100 probes: In order to investigate the MSI performance of the probes, the P-100 was applied to conduct AFA-DESI-MSI analysis on the vertical plane sections of rat brain tissues, and the results are shown in Fig. 2. As shown in Fig. 2A, it can be observed that numerous metabolites can be detected in the represented spectrum, including amino acids, carnitines, nucleotides, *etc*., in the mass range from 100 to 500, also with lipids in the mass range from 700 to 900 [46]. This means high coverage metabolites mapping for MSI can be achieved by this P-100 probe. In addition, the application of MSI technology based on this probe can also clearly show the spatial distribution information of some low-abundance metabolites in the rat brain (Fig. 2B), such as *m*/*z* 857.5848 (ion intensity 3E2), *m*/*z* 661.5161 (ion intensity 1E2), and *m*/*z* 448.3420 (ion intensity 2E2) with ion intensities more than or equal to three orders of magnitude (ion intensity, 4E6, Fig. 2A). In Fig. 2C, the two endogenous metabolite ions at *m*/*z* 126.0317 and *m*/*z* 126.0221 showed different spatial distributions with a $\Delta m/z$ of only 0.01 Da, of which *m*/*z* 126.0317 was evenly distributed in the brain section and *m*/*z* 126.0220 was mainly distributed in the microregions except for the middle brain (MB), thalamus (TH), PN and MD; The superimposed image of the specific ions at *m*/*z* 734.5692, *m*/*z* 746.6060 and *m*/*z* 140.0684 characterized by different colors can clearly and accurately show microregions of brain tissue (Fig. 2D). In Fig. 2E, a spatial resolution with 70 μm on the cerebellar medulla can be observed. Furthermore, as shown in Fig. 2F, a lot of unique metabolites can be observed with their specific distribution pattern in the brain section.

As shown in Fig. S2 (Supporting information), the performance on MSI of a coronal rat brain section further demonstrated that the P-100 probe can acquire high quality MSI image of *m*/*z* 104.0708, and has advantage than a commercial ESI sprayer. Commercial or hand-made ESI sprayer was always used as an ionization probe for DESI-MS/MSI analysis due to its widely usage and accessibility [45]. Herein, these AFA-DESI probes were designed with a unique long and cylindrical sprayer nozzle (Fig. S2A) but not the general conical ESI sprayer nozzle. Therefore, they can form more focused spray plume and smaller diameter action spots on the sample surface. The above results showed that MSI technology based on the P-100 probe can efficiently desorb and ionize the endogenous metabolite from tissues section, thereby achieving high-coverage, high-sensitivity, and reasonable spatial resolution (less than 100 μm).

To verify the application of the probe for spatially resolved metabolomics, we further used it to analyze tumor tissues. The results in Fig. 3 showed that AFA-DESI-MSI analysis based on P-100 can accurately obtain the metabolic profile of cancerous, paracancerous, and normal areas. The overlay image of *m*/*z* 255.0627 and *m*/*z* 267.1564 ions (cancerous area: red, paracancerous area:

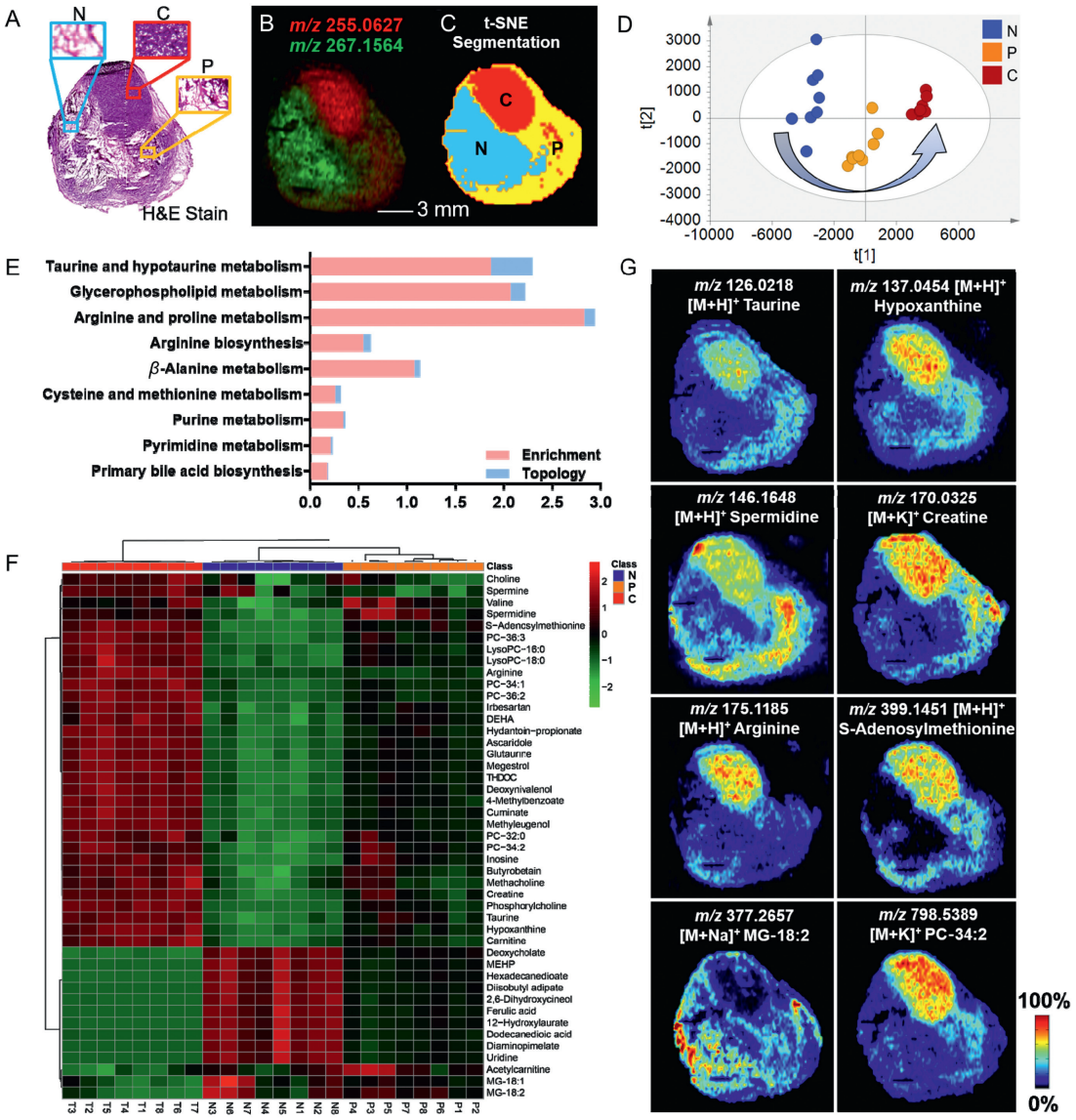

Fig. 3. AFA DESI-MSI and spatially resolved metabolomics analysis results of tumor tissue using the P-100 probe. (A) H&E staining image of tumor tissue. (B) A superimposed MS image of *m/z* 255.0627 and *m/z* 267.1564 ions. (C) The t-SNE spatial segmentation of the tumor microregion based on metabolite profiling. (D) Principal component analysis (PCA) score plots generated with data from the normal area, paracancerous area, and cancerous area. (E) Pathway analysis of differential metabolites of different areas in tumor tissue. The bar chart is a combination of enrichment *P*-values (blue bars) and topological analysis (red bars) of the pathways denoted on the *y* axis. (F) Hierarchical clustering and heat map analysis of differential metabolites. (G) MS images of representative metabolites. N, normal area; P, paracancerous area; C, cancerous area.

superimposed red and green, and normal area: green) (Fig. 3B) showed the same pathological characteristics as the H&E staining (Fig. 3A). Furthermore, the t-SNE method [47] was used to realize the fine division of tumor tissues based on the overall metabolic profile, and more subtle differences in the heterogeneous structure were found (Fig. 3C). We examined the data from the normal area, paracancerous area, and cancerous area with PCA, which showed distinct profiles between the different areas with a gradual increasing trend (Fig. 3D). Orthogonal partial least squares-discriminant analysis (OPLS-DA) with a "cross-comparison scheme" was used to screen differential metabolites (Fig. S3 in Supporting information), and 45 differential metabolites (Variable important in projection VIP > 1, *P*-value < 0.05) with significant changes in three comparison groups were identified (Table S2 in Supporting information). Then, pathway analysis (Metaboanalyst 5.0), including functional enrichment and pathway topological analysis, was used to discover significantly altered metabolic pathways, such as taurine and hypotaurine metabolism, glycerophospholipid metabolism, arginine, and proline metabolism (Fig. 3E). Altered metabolites were further processed for clustering, and the generated heatmap significantly revealed the relative abundance in different areas (Fig. 3F). Most metabolites showed a gradual increasing trend from normal to adjacent to cancerous areas, such as amino acids and derivatives, lipids, amines, and nucleosides. A few metabolites, mostly organic acids and their derivatives, were downregulated. The MSI images of some differential metabolites are shown in Fig. 3G. Among them, taurine, hypoxanthine, spermidine, creatine, *S*-adenosylmethionine, and phosphatidylcholine (PC 34:2) were upregulated in both the cancerous area and paracancerous area, while arginine was upregulated only in the cancerous area. MG-18:2 was downregulated in the tumor area. The use of P-100 probe can provide higher sensitivity and high specificity analysis results for spatially resolved metabolomics research of tumor-like heterogeneous tissues, thereby providing a more accurate molecular basis for tumor

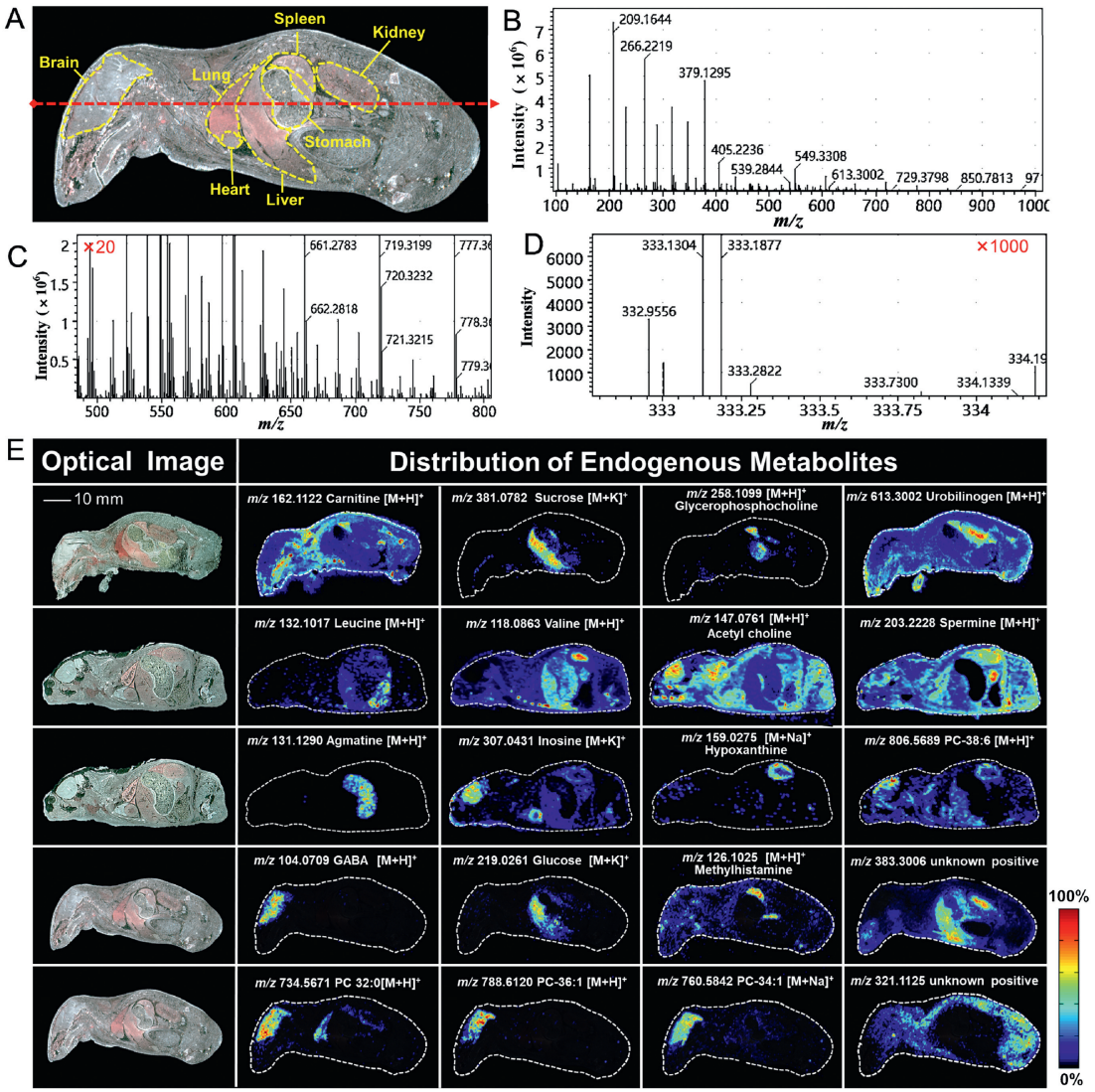

Fig. 4. The AFA-DESI-MSI analysis results of the whole-body section of mouse using the P-200. (A) The optical image of the whole-body animal sample. (B) Average mass spectra of whole-body MSI in positive mode; (C) 20-fold magnification at *m/z* 500-800; (D) 1000-fold magnification at *m/z* 332 within 1.0 Da width. (E) MS images of representative metabolites.

metabolism research and molecular pathological diagnosis of cancer.

MSI analysis of whole-body tissue section using P-200: The whole-body sections of mice were analyzed by AFA-DESI-MSI with the P-200 at 0.5 mm per pixel (Fig. 4A). In positive ion mode, the highest intensity of endogenous metabolite ion was about 4E6. Some small-molecule metabolite (*m/z* 100-400), lysophospholipids (*m/z* 450~600), and phospholipids (*m/z* 600-900) all showed higher intensity (Fig. 4B). After magnifying the ordinate of intensity by 20 times (Fig. 4C) and 1000 times (Fig. 4D), the ion peaks of a variety of low-abundance metabolites still can be observed, indicating that the probe was better for desorption and ionization of large-sized tissue samples with rough spatial resolution, and can analyze endogenous metabolites in whole-body animals with high sensitivity. The MSI image of representative endogenous metabolites in Fig. 4E clearly showed the spatial distribution of each metabolite in the whole-body mouse. Carnitine, glycerophosphocholine, and methylhistamine have the highest contents in the spleen. Valine, spermine, urobilinogen, and hypoxanthine were mainly distributed in the kidney, and the contents of valine and urobilinogen were higher in the renal medulla, especially, while hypoxanthine was mainly distributed renal cortex. The contents of inosine, γ-aminobutyric acid (GABA), acetylcholine, and some phosphatidylcholines (PC 38:6, PC 32:0, PC 34:1, and PC 36:1) were higher in the brain, and inosine and PC 38:6 were also distributed in the liver and renal cortex, while PC 32:0 was higher in the lung. In addition, agmatine was mainly found in the stomach; the metabolite ion *m/z* 321.1125 was distributed in the muscle outside the organ.

The organ-specific distribution of the above metabolites indicated that the P-200 can achieve high-sensitivity and high-specificity analysis of endogenous metabolites in whole-body animals. The uniform and specific distribution of the metabolites in the corresponding organs confirmed the stable spray of the probe and the excellent reproducibility of desorption and ionization. In particular, the ability to distinguish tissue micro-regions such as the renal cortex and renal medulla indicated its higher resolution. It is expected to provide an intuitive research tool for the pharmacological and toxicological evaluation of drugs by using the whole-body MSI analysis technology based on the large-size probe.

In this study, we achieved two types of DESI probes to improve the performance of ambient MSI for spatially resolved

metabolomics. The laser photomicrograph experiment demonstrated the differential adaptability of the two probes with different spray flow rates. The AFA-DESI-MSI analysis of biotissue sections using these probes demonstrated that the sensitivity was greatly improved to realize desorption and ionization of low-abundance metabolites and obtained a satisfactory spatial resolution for spatially resolved metabolomics analysis. The imaging experiments of rat brain tissue sections and whole-body tissue sections showed that the use of these probes can better characterize the spatial distribution of metabolites, which fully meets the requirements of high sensitivity and high specificity. The spatially metabolomics studies on tumor tissues have found region-specific differential metabolites, most of which were upregulated in the cancerous area, mainly distributed in pathways such as taurine and hypotaurine metabolism, glycerophospholipid metabolism, arginine, and proline metabolism. As the core procedure of the AFA-DESI-MSI analysis, desorption ionization with these probes can achieve multifaceted improvements and further expand its application in spatially resolved metabolomics, thereby promoting research on disease diagnosis, biomarker discovery and pathological mechanisms.

Declaration of competing interest

The authors declare no competing financial interest.

Acknowledgments

The authors would like to thank financial support from the National Natural Science Foundation of China (Nos. 81974500 and 81773678), and the CAMS Innovation Fund for Medical Sciences (No. 2022-I2M-2-001).

Supplementary materials

Supplementary material associated with this article can be found, in the online version, at doi:10.1016/j.cclet.2022.107865.

References

[1] T. Alexandrov, Annu. Rev. Biomed. Data Sci. 3 (2020) 61–87.
[2] Z. Takáts, J.M. Wiseman, B. Gologan, R.G. Cooks, Science 306 (2004) 471–473.
[3] A.R. Buchberger, K. DeLaney, J. Johnson, L. Li, Anal. Chem. 90 (2018) 240–265.
[4] Q. Wu, S.S. Rubakhin, J.V. Sweedler, Anal. Chem. 92 (2020) 6613–6621.
[5] J.J. He, Z.G. Luo, L. Huang, et al., Anal. Chem. 87 (2015) 5372–5379.
[6] D.J. Ryan, J.M. Spraggins, R.M. Caprioli, Curr. Opin. Chem. Biol. 48 (2019) 64–72.
[7] O. Karlsson, J. Hanrieder, Arch. Toxicol. 91 (2017) 2283–2294.
[8] P. Abramowski, O. Kraus, S. Rohn, et al., Cancer Genom. Proteom. 12 (2015) 179–187.
[9] C. Zhao, T. Yong, Y.B. Zhang, et al., Environ. Int. 135 (2020) 105378.
[10] Y.H. Kim, Y. Fujimura, T. Hagihara, et al., Sci. Rep. 3 (2013) 2805.
[11] Q.W.J. Cao, Y.J. Wang, B.M. Chen, et al., ACS Chem. Neurosci. 10 (2019) 1222–1229.
[12] J.L. Zhang, J. Rector, J.Q. Lin, et al., Sci. Transl. Med. 9 (2017) ann3968.
[13] E. Fridjonsdottir, R. Shariatgorji, A. Nilsson, et al., Sci. Adv. 7 (2021) eabe5948.
[14] J.H. Zhang, Y.J. Hong, P.S. Xie, et al., Front. Pharmacol. 11 (2020) 593815.
[15] S.H. Yang, H.H. Liu, X. Huang, et al., Int. J. Mass Spectrom. 434 (2018) 93–99.
[16] D. Calligaris, D.R. Feldman, I. Norton, et al., Int. J. Mass Spectrom. 377 (2015) 690–698.
[17] S. Schulz, M. Becker, M.R. Groseclose, et al., Curr. Opin. Biotechnol. 55 (2019) 51–59.
[18] L.P. Zhan, X. Huang, J.J. Xue, et al., Food Chem. 338 (2021) 127984.
[19] J.M. He, C.L. Sun, T.G. Li, et al., Adv. Sci. 5 (2018) 1800250.
[20] H. Liebl, J. Appl. Phys. 38 (1967) 5277–5283.
[21] K. Li, J. Liu, C.R.M. Grovenor, K.L. Moore, Annu. Rev. Anal. Chem. 13 (2020) 273–292.
[22] F. Hillenkamp, E. Unsöld, R. Kaufmann, R. Nitsche, Nature 256 (1975) 119–120.
[23] D. Weibel, S. Wong, N. Lockyer, et al., Anal. Chem. 75 (2003) 1754–1764.
[24] S.S. Rubakhin, A. Ulanov, J.V. Sweedler, J. Am. Soc. Mass. Spectrom. 26 (2015) 958–966.
[25] P.J. Hart, M.R. Clench, MALDI-MSI of lipids in human skin, in: L. Cole (Ed.), Imaging Mass Spectrometry. Methods in Molecular Biology, vol. 1618, Humana Press, New York, 2017, pp. 29–36.
[26] H.X. He, L. Qin, Y.M. Zhang, et al., Anal. Chem. 91 (2019) 2634–2643.
[27] A.D. Feenstra, M.E. Dueñas, Y.J. Lee, J. Am. Soc. Mass. Spectrom. 28 (2017) 434–442.
[28] Q. Wu, J.L. Chu, S.S. Rubakhin, et al., Chem. Sci. 8 (2017) 3926–3938.
[29] K. Nozaki, Y. Nakabayashi, T. Murakami, et al., J. Mass Spectrom. 54 (2019) 612–619.
[30] M. Fresnais, W.E. Haefeli, J. Burhenne, R. Longuespée, OMICS 24 (2020) 53–54.
[31] S. Gerbig, H.E. Brunn, B. Spengler, S. Schulz, Anal. Bioanal. Chem. 407 (2015) 7379–7389.
[32] A.M. Gouw, K. Margulis, N.S. Liu, et al., Cell Metab 30 (2019) 556–572.e5.
[33] J.M. He, F. Tang, Z.G. Luo, et al., Rapid Commun. Mass Spectrom. 25 (2011) 843–850.
[34] Y.W. Lv, T.G. Li, C.G. Guo, et al., Chin. Chem. Lett. 30 (2019) 461–464.
[35] Z.G. Luo, J.M. He, Y. Chen, et al., Anal. Chem. 85 (2013) 2977–2982.
[36] X.W. Song, Z.G. Luo, X. Li, et al., Anal. Chem. 89 (2017) 6318–6323.
[37] Z.H. Wang, B.S. He, Y.Q. Liu, et al., Acta Pharm. Sin. B 10 (2020) 1083–1093.
[38] X.W. Song, J.M. He, X.C. Pang, et al., Anal. Chem. 91 (2019) 2838–2846.
[39] J. Zhang, Q.Q. Du, X.W. Song, et al., Theranostics 10 (2020) 2621–2630.
[40] D. Liu, J. Huang, S. Gao, et al., Acta Pharm. Sinica B 12 (2022) 3341–3353.
[41] X.X. Mao, J.M. He, T.G. Li, et al., Sci. Rep. 6 (2016) 21043.
[42] T.G. Li, J.M. He, X.X Mao, et al., Sci. Rep. 5 (2015) 14089.
[43] L.J. Huang, X.X. Mao, C.L. Sun, et al., Molecules 27 (2022) 1390.
[44] C.L. Sun, T.G. Li, X.W. Song, et al., Proc. Natl. Acad. Sci. U. S. A. 116 (2019) 52–57.
[45] D.I. Campbell, C.R. Ferreira, L.S. Eberlin, R.G. Cooks, Anal. Bioanal. Chem. 404 (2012) 389–398.
[46] J.M. He, L.J. Huang, R.T. Tian, et al., Anal. Chim. Acta 1015 (2018) 50–57.
[47] L.V.D. Maaten, G. Hinton, J. Mach. Learn. Res. 9 (2008) 2579–2605.